Available online at www.sciencedirect.com
ScienceDirect
Geochimica et Cosmochimica Acta 74 (2010) 1485–1497
Geochimica et Cosmochimica Acta
www.elsevier.com/locate/gca

Adsorption of Sr^{2+} and Ba^{2+} at the cleaved mica–water interface: Free energy profiles and interfacial structure

Artur Meleshyn *

Center for Radiation Protection and Radioecology (ZSR), Leibniz Universität Hannover, Herrenhäuser Str. 2, 30419 Hannover, Germany

Received 21 September 2009; accepted in revised form 10 December 2009; available online 24 December 2009

Abstract

Monte Carlo simulations show that the adsorption position of the Sr^{2+} or Ba^{2+} ion on the cleaved muscovite surface is determined by the radius of the ion's first hydration shell, hydrogen bonding of the first shell water molecules with the basal oxygens of muscovite as well as a requirement of minimization of the number of muscovite's lattice cations in the ion's first coordination shell. Accordingly, Sr^{2+} or Ba^{2+} adsorbs in ditrigonal cavities at a distance of 1.12 Å or 1.35 Å, respectively, from the basal surface on dehydrated mica and above tetrahedral substitutions at a height of 1.93 ± 0.02 Å or 2.15 ± 0.03 Å, respectively, at the highest simulated water coverage of 28 H_2O per ion. The ion's displacement from a ditrigonal cavity occurs upon adsorption of 2 H_2O per ion for Sr^{2+} and 3 H_2O per ion for Ba^{2+}. At a coverage of 28 H_2O per ion, outer-sphere adsorption of Sr^{2+} or Ba^{2+} at a height of 3.9 ± 0.2 Å or 4.17 ± 0.07 Å, respectively, is possible albeit unfavorable on the free energy scale by 107 ± 7 kJ/mol or 89 ± 13 kJ/mol, respectively, as compared to inner-sphere adsorption. Activation energies for the transformation between inner-sphere and outer-sphere adsorptions are calculated to be 121 ± 3 kJ/mol for Sr^{2+} and 99 ± 10 kJ/mol for Ba^{2+}. A comparison of these values with those reported recently for Mg^{2+} and Ca^{2+} results in an adsorption affinity sequence $Mg^{2+} > Ca^{2+} > Sr^{2+} > Ba^{2+}$ in agreement with the sequence predicted recently for low dielectric constant solids (which include mica) (Sverjensky, 2006). A recent resonant anomalous X-ray reflectivity study of Sr^{2+} adsorption on muscovite (Park et al., 2006) has questioned the common assumption (Stumm, 1992), which is supported by the present simulation results, that inner-sphere adsorption is stronger than outer-sphere adsorption. A modification of the cleaved muscovite surface as a result of Sr^{2+} adsorption in muscovite's ditrigonal cavities and related destabilization of muscovite's hydroxyl groups is proposed as a possible reason for this controversy.

1. INTRODUCTION

Understanding the Sr^{2+} and Ba^{2+} adsorption at mineral–water interfaces still remains a challenging and controversial issue in geochemical science despite considerable attention in the past two decades. Notwithstanding their indisputable affinity to environmentally and industrially important smectites, illites, and micas, which carry a permanent negative lattice charge and have very similar structures of the basal surface, there is a strong disagreement on the strength of this affinity. From surface force apparatus (Pashley and Israelachvili, 1984) and X-ray absorption fine structure spectroscopy studies (Chen and Hayes, 1999; Cole et al., 2000) carried out at ion concentrations below ~1 mM, it has been concluded that only weak adsorption of Sr^{2+} and Ba^{2+} as outer-sphere complexes occurs on clay minerals belonging to these three groups. On the contrary, strong adsorption of Sr^{2+} and Ba^{2+} as inner-sphere complexes along with their outer-sphere adsorption has been concluded from X-ray absorption fine structure (Zhang et al., 2001), X-ray reflectivity (XR) (Schlegel et al., 2006; Lee et al., 2007), and resonant anomalous X-ray reflectivity (RAXR) (Park et al., 2006) spectroscopy studies carried out at ion concentrations above ~5 mM. Albeit low applied concentrations may be a reason for the observation of weak adsorption of these alkaline earth ions, as a compensation

* Tel.: +49 511 762 3069; fax: +49 511 762 170917.
E-mail address: meleshyn@zsr.uni-hannover.de

0016-7037/$ - see front matter © 2009 Elsevier Ltd. All rights reserved.
doi:10.1016/j.gca.2009.12.019

of the mica lattice charge by inner-sphere adsorbed Ca^{2+} has been found to occur at higher $CaCl_2$ concentrations of ~10 mM (Scales et al., 1990; Schlegel et al., 2006), the recent experimental results for Sr^{2+} adsorption on mica have not really contributed to a final resolution of the controversy. Indeed, ion-specific electron density profiles for Sr^{2+} measured with RAXR in the direction perpendicular to the muscovite–water interface have revealed equivalent occupancies of inner-sphere and outer-sphere adsorption positions by Sr^{2+} with the total occupancy corresponding to that necessary to compensate the negative charge of muscovite lattice (Park et al., 2006, 2008). The logical conclusion from this observation about the equivalence of inner-sphere and outer-sphere adsorption strengths contradicts the common assumption (Stumm, 1992), however, as has been admitted by Park et al. (2006). Notably, the results for Rb^+ adsorption on the cleaved muscovite surface in the same studies by Park et al. (2006, 2008) agree with the common assumption that inner-sphere adsorption is stronger than outer-sphere adsorption (Stumm, 1992).

Here, the results of Monte Carlo (MC) simulations with the Metropolis algorithm for sampling structural properties and the Wang–Landau algorithm (Wang and Landau, 2001) for sampling free energy profiles in the direction perpendicular to the mineral surface on dehydrated as well as hydrated Sr^{2+}– and Ba^{2+}–muscovites are presented. Following the experimental procedure applied previously to study interfacial properties of the cleaved muscovite in dependence on increasing water film thickness controlled by air humidity (Beaglehole et al., 1991; Xu and Salmeron, 1998a,b), the cleaved muscovite surface with incrementally increasing water coverages is considered in the present study to examine changes in adsorption positions and hydration structures of adsorbed Sr^{2+} and Ba^{2+} ions up to a water film thickness corresponding to a relative air humidity of 95–100% (Beaglehole et al., 1991). The simulated system is configured following the model of the process studied in the X-ray experiments (Schlegel et al., 2006; Park et al., 2006, 2008; Lee et al., 2007), which states that (1) Sr^{2+} or Ba^{2+} adsorption from (2) aqueous solution occurs on (3) the cleaved muscovite surface. The calculated free energy characteristics of Sr^{2+} and Ba^{2+} adsorption are discussed in the context of the experimental studies in order to help clarify the existing controversy on adsorption of alkaline earth ions at the cleaved mica surface.

2. SIMULATION DETAILS

The simulation cell with lateral dimensions of ~20.75 Å × ~18.01 Å and a thickness of 116.6 Å encloses eight unit cells of $2M_1$-muscovite mica with the formula unit $KAl_2(Si_3Al)O_{10}(OH)_2$ (unit cell area $A_{uc} = 46.72$ Å^2) and a vacuum slab of 100 Å as measured between the basal oxygens of the cleaved surfaces (Fig. EA-1 in electronic annex). Al substitutions in tetrahedral sheets of muscovite layers are arranged in accordance with Löwenstein's rule of avoidance of Al–O–Al linkages, so that hexagonal rings of Si_4Al_2 and Si_5Al_1 compositions are equally represented in the modeled mica layer (Fig. 1a). Six basal oxygen atoms bridging Si and Al atoms of the same hexagonal ring are in

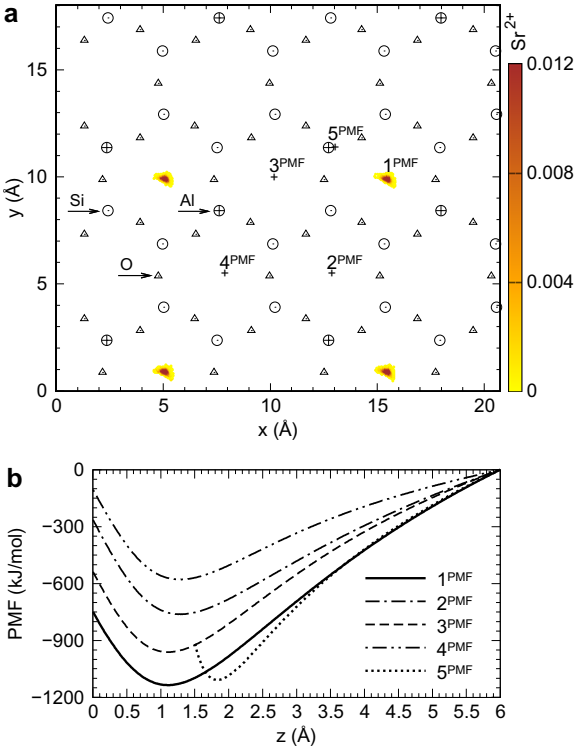

Fig. 1. Lateral density of Sr^{2+} (atoms/Å^2, color box) sampled with the Metropolis algorithm (a) and PMF profiles (kJ/mol) as functions of the distance between Sr^{2+} and mica (b) for the dehydrated muscovite surface. For muscovite, only structural ions and basal oxygens of the tetrahedral sheet at the interface with vacuum are shown in (a). Equilibrium positions of Sr^{2+} ions are not exactly above the tetrahedral substitutions because of a depression by 0.22 Å (Schlegel et al., 2006) of one of the three basal oxygens bonded to a tetrahedral substitution. Five different PMF paths are considered in (b): above the equilibrium Sr^{2+} position (denoted 1^{PMF}), above ditrigonal cavity centers closer to the other adsorbed Sr^{2+} ions (marked by a "+" symbol and denoted 2^{PMF}, 3^{PMF}, and 4^{PMF}), and above a neighboring tetrahedral substitution (denoted 5^{PMF}). The position of the basal oxygens of muscovite was set to $z = 0$ Å. PMF profiles were arbitrarily set to zero at $z = 6$ Å.

the vertices of the two equilateral triangles with side lengths of ~4 Å and ~5 Å featuring a ditrigonal cavity in the muscovite surface (Kuwahara, 2001). Atomic positions and parameters of the muscovite unit cell were taken from an XR study (Schlegel et al., 2006).

To simulate thin water films adsorbed on the cleaved surface of Sr^{2+}- and Ba^{2+}-exchanged muscovites, i water molecules per A_{uc} ($i = 2$–6, 8, 12, 14) were randomly distributed in a slab near one of the cleaved mica surfaces, at which K^+ ions were replaced by 0.5 Sr^{2+}/A_{uc} or 0.5 Ba^{2+}/A_{uc} in accordance with the experimental procedure, in which K^+ is completely exchanged from the cleaved muscovite surface (Schlegel et al., 2006; Park et al., 2008). To examine the dependence of the interfacial solution structure on Ba^{2+} coverage, the cleaved muscovite–water interface with 0.125, 0.25, and 0.5 Ba^{2+}/A_{uc} were simulated additionally at the maximum water coverage (0.75 or 0.5 H_3O^+/A_{uc}

were added at the muscovite–water interface for the two lowest coverages in order to compensate the muscovite lattice charge). Water oxygen or basal oxygen is considered as an acceptor A of a hydrogen bond from a water molecule when the separation between the water oxygen and the acceptor is less than 3.5 Å and the H–O···A angle is less than 30° (Ferrario et al., 1990).

The MC simulations were carried out in a constant-NVT ensemble at 298 K. The TIP4P model (Jorgensen et al., 1983) was used for water and a TIP4P-based model (Gertner and Hynes, 1998) was used for H_3O^+. OPLS-AA force field equations and potential parameters (Jorgensen et al., 1996) along with the procedure by Skipper et al. (1995) for rigid mineral layers were applied to calculate potential energies of interactions. The imposed rigidity of the mica layers is a reasonable approximation considering that mineral atoms show relaxations of <0.05 Å at the interface between muscovite and deionized or $BaCl_2$ solutions and ~0.01 Å within the mineral layer (Cheng et al., 2001; Lee et al., 2007). Three-dimensional boundary conditions, a cut-off distance of 9 Å and the all-image convention were adopted for the short-range interactions, and the Ewald technique as modified for systems with slab geometry (Yeh and Berkowitz, 1999) was applied to handle the long-range Coulomb interactions.

In the first step, the Metropolis algorithm was employed for the sampling of structural properties with a mean of $\sim 1.4 \times 10^6$ MC cycles (a trial displacement of all interfacial cations as well as a trial displacement or rotation of all water molecules were attempted during one MC cycle) used for equilibration and a mean of $\sim 2 \times 10^4$ MC cycles used for sampling. In the second step, the expanded ensemble density of states (EXEDOS) method (Kim et al., 2002) based on the Wang–Landau algorithm (Wang and Landau, 2001) was applied to the equilibrated systems for the calculation of the potential of mean force (PMF) between interfacial cation and mica. For this purpose, three of four interfacial cations in the simulation cell were fixed in their equilibrium positions, whereas one interfacial cation was allowed to move along a line normal to the mineral surface and intersecting the equilibrium lateral position of this cation obtained in the preceding Metropolis Monte Carlo run (Fig. 1a). Its distance z from the surface (height) was allowed to change in the ranges 1.6–6 Å (1.5–6 Å on dehydrated mica) for Sr^{2+} or 1.85–6 Å (1.7–6 Å on dehydrated mica) for Ba^{2+} in the equilibrium positions above a tetrahedral substitution as well as in the ranges 0–6 Å for Sr^{2+} and Ba^{2+} in the equilibrium positions above a ditrigonal cavity center.

For water coverages in the range 2–4 H_2O/A_{uc}, a second PMF path was considered in addition to the equilibrium positions. For this purpose, if the latter was above a ditrigonal cavity center (1^{PMF} in Fig. 1a), the same cation was displaced into the position above a neighboring tetrahedral substitution (5^{PMF} in Fig. 1a) and vice versa. On dehydrated mica, three further PMF paths were considered, in which an interfacial cation was displaced from its interfacial position above a ditrigonal cavity center (1^{PMF} in Fig. 1a) into positions above centers of neighboring ditrigonal cavities (2^{PMF}, 3^{PMF}, and 4^{PMF} in Fig. 1a).

The Wang–Landau acceptance ratio $\min\{1, \exp(-(U_{new} - U_{old})/kT - (\ln g_{new} - \ln g_{old}))\}$ was applied for trial moves with interfacial cations, where densities of state $g(z)$ were initially set to $e^{0.1}$ for all z in the considered range (divided into bins with the width $\Delta z = 0.01$ Å). Water molecules were allowed to rearrange through arbitrary trial moves with the Metropolis acceptance ratio $\min\{1, \exp(-(U_{new} - U_{old})/kT)\}$. After each trial move of the interfacial cation (one per MC cycle), the density $g(z)$ of the corresponding state z was updated by a convergence factor f (set initially to $e^{0.1}$). After each state was visited at least $100/(\ln f)^{1/2}$ times (Zhou and Bhatt, 2005), $\ln f$ was halved, and a new EXEDOS cycle was started. A simulation was run for five EXEDOS cycles, sufficient for the calculation of free energy profiles for a single or several reaction coordinates at a fixed temperature (Kim et al., 2002). The PMF $-kT \ln g(z)$ representing the free energy profile in the direction perpendicular to the surface was calculated at the end of the simulation. For water coverages in the range 5–14 H_2O/A_{uc}, free energy profiles for all four interfacial cations in the simulated cell were calculated in four parallel simulation runs in order to calculate average free energy profiles and average free energy characteristics of Sr^{2+} and Ba^{2+} adsorption on the cleaved muscovite surface.

The applied procedure prevents a relaxation of the distribution of three interfacial ions upon sampling of the free energy profile for the fourth one. However, it should be kept in mind that the primary interest of this study is the free energy difference between the first and the second minima of the free energy profiles, which correspond to the inner-sphere and outer-sphere adsorptions. If the depth of the first or second minimum with respect to the state at 6 Å (which is the sampled state most distant from the surface) is to be determined most precisely, the state, in which all interfacial ions are in their most favorable adsorption state, should be involved. Importantly, the applied algorithm uses a predefined reaction path, which is not necessarily identical to the (unknown) experimental one, and prescribes that an ion follows this path five times (five EXEDOS cycles away from the surface and back). Therefore, it should be provided that the possible ion relaxation at the algorithm's step, at which the chosen ion is far from the surface, does not prevent or strongly disfavor its return to the original most favorable adsorption position. An important example of such a relaxation is that the three ions remaining at the surface rearrange to increase the mutual separations (which is favorable as shown in Section 3.1). As a result, the ion, which is up to 6 Å away from the surface, will need to return in a very different structure on the muscovite surface with either (1) the previously free neighboring adsorption site being occupied or (2) its previous adsorption site being occupied as a result of the ion distribution relaxation. Since the reaction path cannot change, both situations would be fatal for the correct sampling of the free energy profile. Classical simulation methods generally represent an approximation to the real system, and in the present study, the fixation of the ion distribution for sampling free energy profiles is one of the necessary approximations.

3. RESULTS AND DISCUSSION

3.1. Adsorption of Sr^{2+} and Ba^{2+} on the dehydrated surface of cleaved mica

A comparison of free energy profiles for Sr^{2+} on the dehydrated surface of cleaved mica (Fig. 1b) shows that differently than the smaller alkaline earth cations Mg^{2+} and Ca^{2+} (Meleshyn, 2009a,b), Sr^{2+} adsorbs preferentially above the center of ditrigonal cavities containing two tetrahedral substitutions (Si_4Al_2 hexagonal ring) at a height (distance from the mica surface) of 1.12 Å (1^{PMF}, Fig. 1a), whereas its adsorption above tetrahedral substitutions at a height of 1.85 Å (5^{PMF}) is less favorable. A match between the hydration radius of Sr^{2+} and the size of mica's ditrigonal cavity is responsible for the preferential Sr^{2+} adsorption in the latter. Indeed, in this position, Sr^{2+} coordinates to three oxygens of the cavity's smaller triangle at a distance of 2.56 Å, which is in very good agreement with the experimental values of 2.56–2.65 Å for the Sr^{2+}–oxygen distance in the first hydration shell (Ohtaki and Radnai, 1993; D'Angelo et al., 1996a; Chen and Hayes, 1999; Seward et al., 1999; Sahai et al., 2000; Moreau et al., 2002), and three more oxygens of the cavity's larger triangle at 3.09 Å (Fig. 2), whereas only three oxygens at 2.44 Å would be coordinated to Sr^{2+} in the position 5^{PMF}. This match compensates for the larger number of positively charged lattice ions in the first coordination sphere of Sr^{2+} with two Al^{3+} and four Si^{4+} ions at distances of 3.46–3.49 Å (Fig. EA-2) in the position 1^{PMF} as compared to only one Al^{3+} and three Si^{4+} ions at distances of 2.51 Å and 3.86 Å, respectively, in the position 5^{PMF}.

Accordingly, for the larger alkaline earth ion Ba^{2+}, the free energy difference between these two adsorption positions is larger than for Sr^{2+}. In the preferred position above the ditrigonal cavity center at a height of 1.35 Å (1^{PMF}, Fig. 3), Ba^{2+} coordinates to three oxygens at a distance of 2.69 Å, which is comparable to the experimental values of 2.78–2.90 Å for the radius of the first hydration shell of Ba^{2+} (Ohtaki and Radnai, 1993; D'Angelo et al., 1996b), to three further oxygens at 3.15 Å and 3.4 Å (Fig. 4) as well as to two Al^{3+} and four Si^{4+} ions at a distance of 3.6 Å (Fig. EA-3). In the position above a tetrahedral substitution at a height of 2.05 Å (5^{PMF}), Ba^{2+} would coordinate to only three oxygens at a less favorable distance of 2.61 Å, as well as to one Al^{3+} and three Si^{4+} ions at distances of 2.73 Å and 4.03 Å, respectively.

It can be further concluded from Figs. 1b and 3b that much the same as for Mg^{2+} (Meleshyn, 2009a) and Ca^{2+} (Meleshyn, 2009b), a random distribution of Sr^{2+} and Ba^{2+} on cleaved mica (2^{PMF}, 3^{PMF}), which would necessarily lead to their adsorption in neighboring Si_4Al_2 or Si_5Al_1 hexagonal rings, is strongly unfavorable as compared to their regular distribution (1^{PMF}). For the considered random distributions, the effect of the hexagonal ring stoichiometry on Sr^{2+} or Ba^{2+} adsorption in a cavity next to the occupied one consists of a strongly increased adsorption

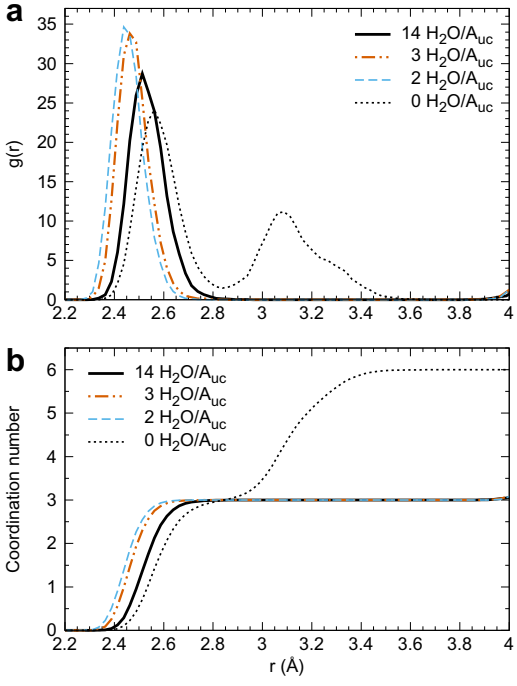

Fig. 2. Radial distributions of basal oxygens as functions of the distance r(Å) from Sr^{2+} adsorbed on the cleaved muscovite surface (a) and corresponding coordination numbers (b). Radial distribution function gives the probability of finding a pair of atoms a distance r apart relative to the probability expected for a completely random distribution at the same density.

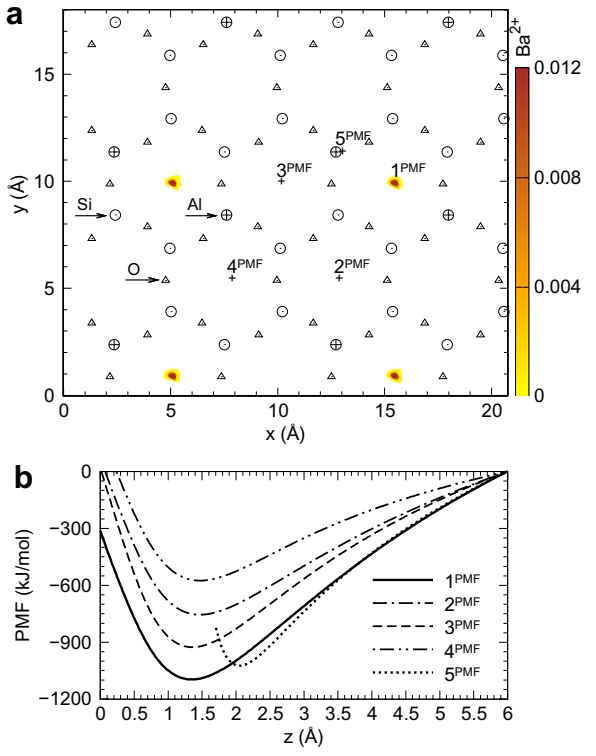

Fig. 3. Lateral density of Ba^{2+} (atoms/Å^2, color box) sampled with the Metropolis algorithm (a) and PMF profiles (kJ/mol) as functions of the distance between Ba^{2+} and mica (b) for the dehydrated muscovite surface. Other details and symbols as in Fig. 1.

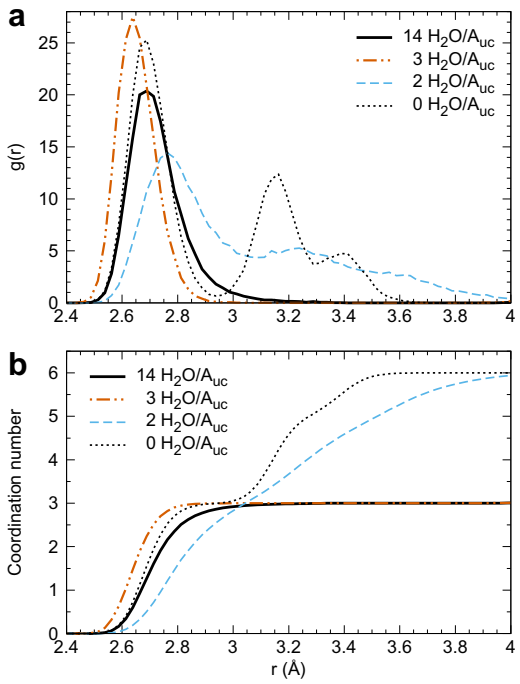

Fig. 4. Radial distributions of basal oxygens as functions of the distance from Ba^{2+} adsorbed on the cleaved muscovite surface (a) and corresponding coordination numbers (b).

height of 1.29–1.32 Å (Sr^{2+}) or 1.47–1.50 Å (Ba^{2+}) for a Si_5Al_1 ring (2^{PMF} and 4^{PMF}) as compared to that of 1.12 Å (Sr^{2+}) or 1.37 Å (Ba^{2+}) for a Si_6Al_2 ring (3^{PMF}). Furthermore, a random distribution with lower mutual separations between adsorbed Sr^{2+} or Ba^{2+} ions (4^{PMF}) is less favorable than that with higher separations (2^{PMF}).

Figs. 1b and 3b reveal that the free energy difference between the specific adsorption state and the state at the height of 6 Å equals 1097 kJ/mol and 1036 kJ/mol for Sr^{2+} and Ba^{2+}, respectively. The electrostatic energy required to separate two layers of K^+–muscovite has been calculated to be ~480 kJ/mol for a separation distance of 6 Å with a simple model as compared to the cleavage energy of ~700 kJ/mol measured in the high vacuum (Giese, 1974). The values calculated in the present study are in line with those reported for K^+, considering that Sr^{2+} and Ba^{2+} have twice the positive charge.

Adsorption heights of Sr^{2+} and Ba^{2+} on the dehydrated surface of cleaved mica can be assumed to be lower than their distances to mica surfaces in the interlayer space because of (1) ion attraction to two opposed mica layers in the latter case and (2) repulsive electrostatic interactions between these layers. In agreement with this assumption, Ba-rich trioctahedral micas are characterized by interlayer Ba^{2+}–mica distances of 1.64–1.71 Å (Brigatti and Poppi, 1993), whereas exchanged dehydroxylated dioctahedral micas also show larger distances of 1.55 Å and 1.67 Å between mica and interlayer Sr^{2+} and Ba^{2+}, respectively (calculated from reported basal spacings (Keppler, 1990) using thicknesses of 2.3 Å for the tetrahedral sheet and 2.1 Å for the octahedral sheet of muscovite). Interestingly, the interlayer Ca^{2+}–mica distance calculated from the same dataset (Keppler, 1990) equals 1.52 Å in a very good agreement with the adsorption height of 1.53 Å for Ca^{2+} on the dehydrated surface of cleaved mica (Meleshyn, 2009b) and seemingly in a contradiction to the above assumption. However, differently than Sr^{2+} and Ba^{2+}, Ca^{2+} adsorbs above tetrahedral substitutions (Meleshyn, 2009b), which obviously allows an effective screening of electrostatic repulsion between opposite mica layers.

3.2. Water layering and hydration of adsorbed ions on cleaved Sr^{2+}– and Ba^{2+}–micas

Exposed to air humidity, muscovite exhibits strong water adsorption with measured water film thicknesses varying between 0.5–0.6 Å at a relative humidity of ~20% up to 7.5–12.5 Å at relative humidities of 95–100% (Beaglehole et al., 1991). This water adsorption leads to the formation of a layer of water molecules singly hydrogen-bonded (H-bonded) to mica at a height of 2.6 Å on Sr^{2+}– and Ba^{2+}–micas (Figs. 5 and 6) much the same as on H_3O^+–, K^+–, and Ca^{2+}–muscovites (Cheng et al., 2001; Wang et al., 2005; Meleshyn, 2008a,b, 2009b). In addition, a minor contribution due to waters (up to 0.75 H_2O/A_{uc}) doubly H-bonded to the surface at 1.7 Å (Fig. 6a, compare to the shoulder at 1.2 Å in Fig. 6b), which have been previously observed for H_3O^+–, K^+–, and Cs^+–muscovites (Wang et al., 2005; Meleshyn, 2008a,b), occurs on Sr^{2+}– and Ba^{2+}–micas at coverages of 12–14 H_2O/A_{uc}. At these water coverages, the formation of the water structure up to a height of 7–7.4 Å is accomplished, and a further water layer at 8–9 Å begins to form (Figs. 5 and 6).

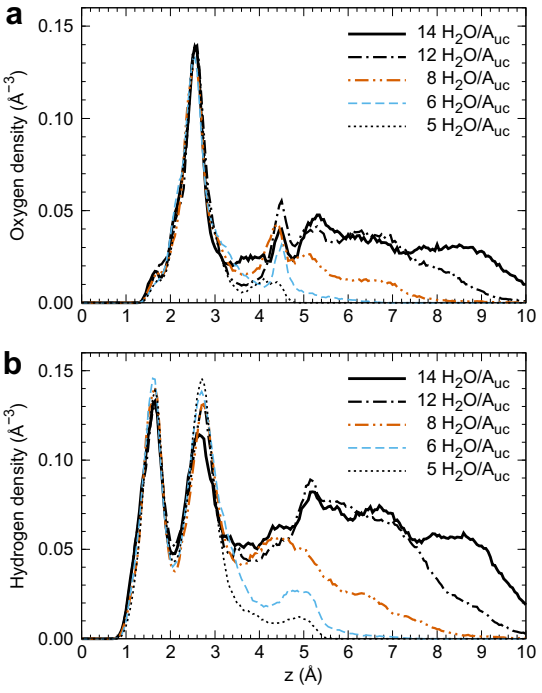

Fig. 5. Water oxygen (a) and water hydrogen (b) atomic density profiles as functions of the distance from the cleaved and Sr^{2+}-exchanged surface of muscovite. The position of the basal oxygens of muscovite was set to $z = 0$ Å.

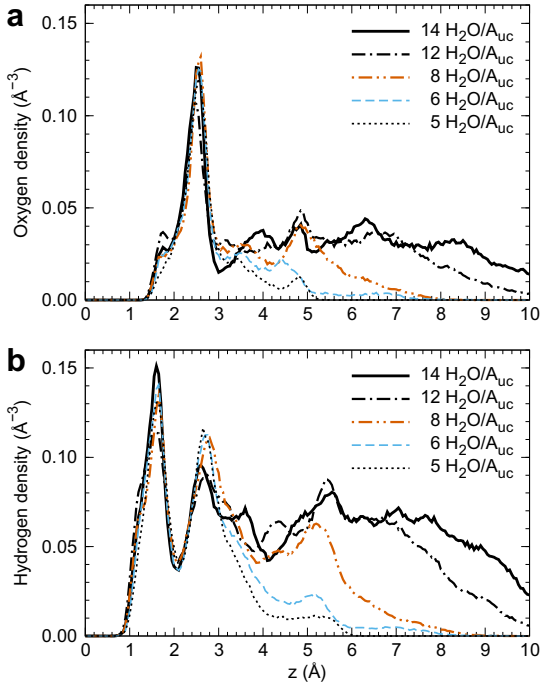

Fig. 6. Water oxygen (a) and water hydrogen (b) atomic density profiles as functions of the distance from the cleaved and Ba^{2+}-exchanged surface of muscovite. The position of the basal oxygens of muscovite was set to $z = 0$ Å.

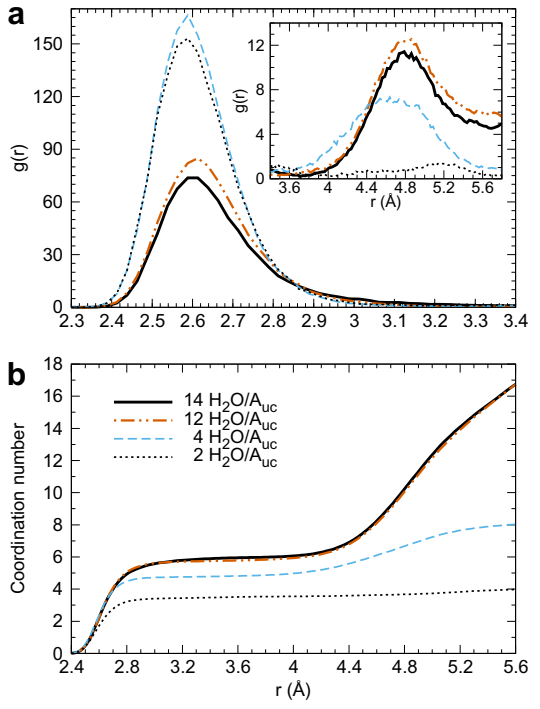

Fig. 7. Radial distributions of water oxygens as functions of the distance from Sr^{2+} adsorbed at the cleaved muscovite–water interface (a) and corresponding coordination numbers (b).

Strong differences in water layering in the height range of 3–5 Å on Sr^{2+}– and Ba^{2+}–micas are related to peculiarities of Sr^{2+} and Ba^{2+} hydrations on mica. Figs. 7 and 8 show that at higher water coverages, the first hydration shell of Sr^{2+} or Ba^{2+} is centered at 2.60 Å or 2.80 Å in a very good agreement with the experimental values of 2.56–2.65 Å (Ohtaki and Radnai, 1993; D'Angelo et al., 1996a; Chen and Hayes, 1999; Seward et al., 1999; Sahai et al., 2000; Moreau et al., 2002) or 2.78–2.90 Å (Ohtaki and Radnai, 1993; D'Angelo et al., 1996b) and consists of 6.0 or 6.5 water molecules, respectively, in addition to three basal oxygens (Figs. 2 and 4). The resulting total coordination numbers of 9.0 and 9.5 agree well with reported experimental values of 7.8–10.3 (Ohtaki and Radnai, 1993; D'Angelo et al., 1996a; Chen and Hayes, 1999; Seward et al., 1999; Sahai et al., 2000; Moreau et al., 2002; Ramos et al., 2003) or 7.8–9.5 (Ohtaki and Radnai, 1993; D'Angelo et al., 1996b) for Sr^{2+} and Ba^{2+}, respectively. The differences in the hydration radii of Sr^{2+} and Ba^{2+} ions account for the differences in the positions of the water layer adsorbed at 4.5 Å and 4.8 Å on Sr^{2+}– and Ba^{2+}–micas, respectively (Figs. 5a and 6a). This layer is very similar to that adsorbed on Ca^{2+}–mica at 4.1 Å in accordance with the even smaller hydration radius of 2.4 Å of the Ca^{2+} ion (Meleshyn, 2009b) and consists of the waters adsorbed in the first hydration shells above adsorbed ions (up to 0.5 H_2O/A_{uc}, see also Fig. EA-4c and EA-4f) as well as of waters singly H-bonded to their first hydration shells (up to 0.5 H_2O/A_{uc}).

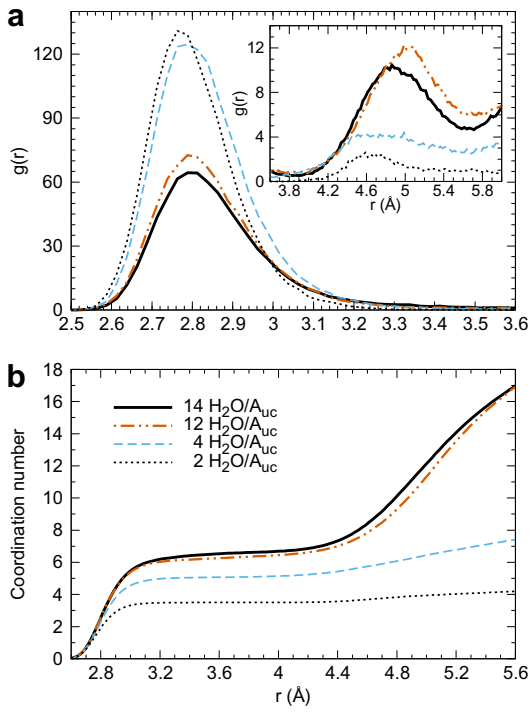

Fig. 8. Radial distributions of water oxygens as functions of the distance from Ba^{2+} adsorbed at the cleaved muscovite–water interface (a) and corresponding coordination numbers (b).

Notably, an intermediate water layer develops on Ba^{2+}–mica at 4.0 Å, unlike Sr^{2+}–mica, starting from a coverage of 8–12 H_2O/A_{uc} and becomes completed at 14 H_2O/A_{uc} (together with the layer at 6.4 Å H-bonded to it) (Fig. 6a).

Its formation is accompanied by an increasing displacement of water hydrogens from positions at 2.8 Å to those at 3.6 Å (Fig. 6b), which is very similar to the previously observed redistribution of water hydrogens between positions at 2.4 Å and 3.2 Å on Mg^{2+}–mica (Meleshyn, 2009a) and occurs as a result of a reorientation of water molecules adsorbed at 2.6 Å to donate H-bonds to next-higher adsorbed water layer(s).

Interestingly, formation of this layer is related to a formation along the crystallographic *b*-direction of a larger scale Ba^{2+} hydration structure of paired hydration shells with coordination numbers (CN) of 6 and 7 as shown in Fig. 9a and b. In each paired shell, six waters are arranged in two triangles centered on an adsorbed Ba^{2+} ion. One triangle consists of waters adsorbed at a height of 2.6 Å and is rotated by 60° with respect to the underlying oxygen triad bonded to an Al substitution. The second triangle is aligned with the oxygen triad and formed either by waters all adsorbed at a height of 4.0 Å (the shell with CN = 6) or by two waters at a height of 4.0 Å and the third one at 2.6 Å (the shell with CN = 7). The seventh water in the latter shell is adsorbed above the Ba^{2+} ion (Fig. 9a and b). The paired shells in this larger scale structure are connected through H-bonding by a water molecule, which is adsorbed at a height of 2.6 Å or 4.0 Å depending on which side of the shell with CN = 6 it resides. The fit between the lengths of connecting H-bonds and the radius of the hydrated Ba^{2+}, on one hand, and the Ba^{2+}–Ba^{2+} distance of ~9 Å, on the other hand, precludes a pairing of two shells with CN = 7 in the crystallographic *b*-direction. The larger Ba^{2+}–Ba^{2+} distance of ~10.3 Å in the *a*-direction, on the contrary, allows such a pairing, which leads to a replication of the paired shells in the *a*-direction. In the hydration shell structure characteristic for specifically adsorbed Sr^{2+} at 12–14 H_2O/A_{uc}, waters adsorbed in the layer at 2.6 Å are arranged in a pentagon, whereas the sixth water molecule adsorbs above the ion much the same as for Ba^{2+} (Fig. 9c and d).

3.3. Adsorption of Sr^{2+} and Ba^{2+} at water coverages of 2–4 H_2O/A_{uc}

Simulation results reveal that already at such a low water coverage as 2 H_2O/A_{uc} for Sr^{2+} or 3 H_2O/A_{uc} for Ba^{2+}, a displacement of ions from adsorption positions in the ditrigonal cavities into those above tetrahedral substitutions occurs. At a coverage of 2 H_2O/A_{uc}, adsorption of Sr^{2+} in ditrigonal cavities (1^{PMF}) at an increased height of 1.30 Å becomes distinctly less favorable than that above tetrahedral substitutions (5^{PMF}) at a height of 1.86 Å (Fig. 10), which results in a corresponding displacement (Fig. EA-4a). On the contrary, adsorption of Ba^{2+} in ditrigonal cavities (1^{PMF}) at an increased height of 1.68 Å remains more favorable compared to that above tetrahedral substitutions (5^{PMF}) at a height of 2.13 Å (Fig. 10), so that no displacement occurs (Fig. EA-4d). At a coverage of 3 H_2O/A_{uc}, however, Ba^{2+} does become preferentially adsorbed above

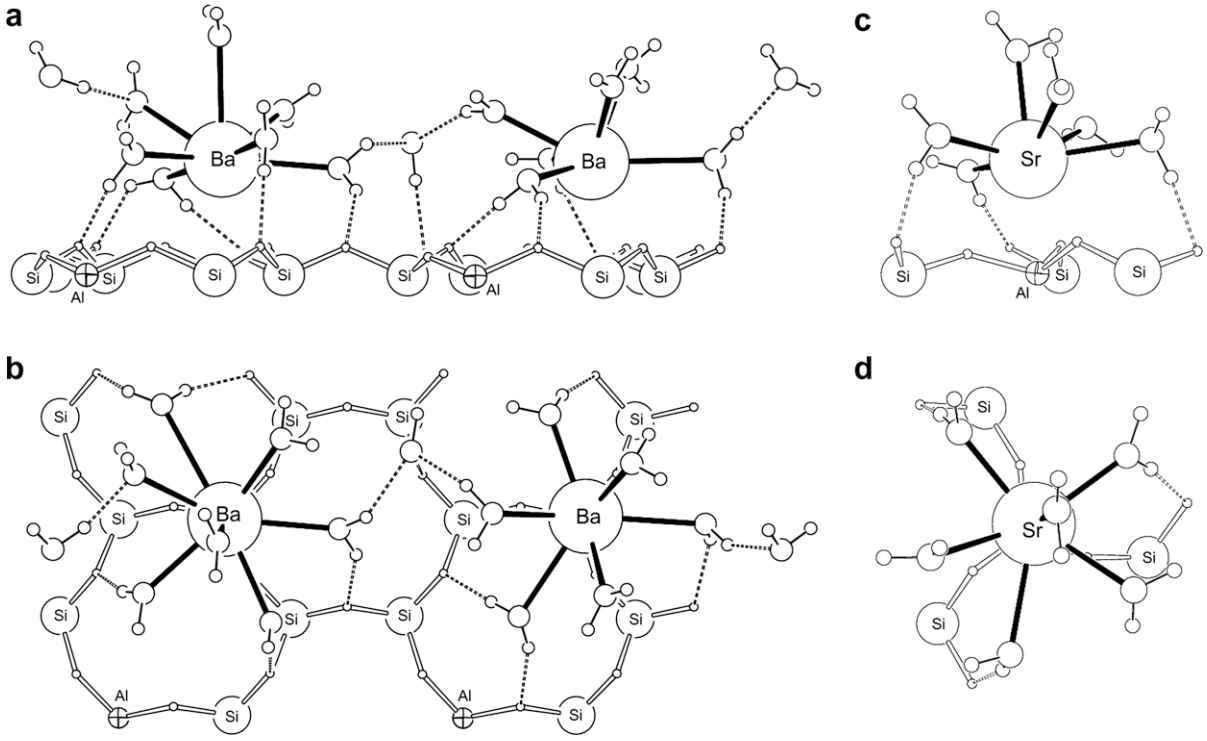

Fig. 9. Snapshots of equilibrium interfacial structures: side (a) and top (b) views of hydrated Ba^{2+} as well as side (c) and top (d) views of hydrated Sr^{2+} on the cleaved muscovite surface at a coverage of 14 H_2O/A_{uc}. Only the first shell water molecules as well as underlying basal oxygens and tetrahedral structural ions are shown. For Ba^{2+}, two water molecules connecting neighboring hydration shells are shown additionally. Bonds between basal oxygens and tetrahedral structural ions are shown as double solid lines. Hydrogen bonds are shown as double dashed lines. Thick sticks connect an ion and its first shell water molecules.

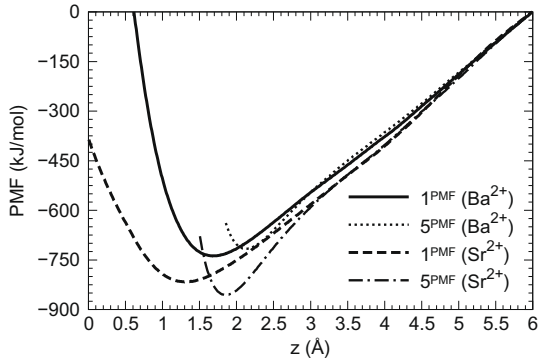

Fig. 10. PMF profiles (kJ/mol) as functions of the distance between Sr^{2+} or Ba^{2+} and muscovite at a coverage of 2 H_2O/A_{uc}. The PMF paths as denoted in Fig. 1a for Sr^{2+} or Fig. 3a for Ba^{2+} are considered. The position of the basal oxygens of muscovite was set to $z = 0$ Å. PMF profiles were arbitrarily set to zero at $z = 6$ Å.

tetrahedral substitutions as well (Fig. EA-4e) at a height of 2.09 Å.

These changes in the adsorption positions of Sr^{2+} and Ba^{2+} occur as a result of a competition between ion hydration and mica hydration. The first process requires that water molecules reside on a sphere with the radius characteristic for the ion's first hydration shell and have positions and orientations, which minimize the unfavorable ion–hydrogen, hydrogen–hydrogen and oxygen–oxygen interactions. The second process requires that adsorption height and lateral position of a water molecule allow it to singly or doubly H-bond to the basal oxygen(s) of mica. Additionally, a requirement of minimization of the number of positively charged lattice ions in the first coordination sphere of the adsorbed ion favors both an increase in the adsorption height and a displacement from a ditrigonal cavity center into a position above a tetrahedral substitution. A mismatch between the first two requirements, which are related to hydration, and the influence of the third one, which is related to ion pairing, lead to changes in lateral and vertical positions of the adsorbed ions.

Indeed, according to the data in Fig. 10, a configuration with three or four water molecules in the first hydration shell like that observed for Ba^{2+} above a ditrigonal cavity center (Fig. EA-4d) is less favorable for Sr^{2+} than another one above a tetrahedral substitution (Fig. EA-4a). Hence, the above discussed mismatch occurs for Sr^{2+} upon its hydration by 3–4 water molecules. Similarly, incorporation of the fifth water molecule into the first hydration shell of the Ba^{2+} ion residing in a ditrigonal cavity is apparently less favorable than a reorganization of the hydration structure upon its displacement from there (compare Figs. EA-4d and EA-4e). Additionally, as a result of such a displacement, the total number of Al^{3+} and Si^{4+} ions coordinated to Sr^{2+} or Ba^{2+} within a radius of 5.2 Å decreases from six to four (Figs. EA-2 and EA-3) with 80% of positive charge residing at a distance increased by 0.5 Å (Figs. EA-2b and EA-3b). An effect of the mismatch between the two hydration processes is demonstrated by the difference in the structure of the first hydration shells of specifically adsorbed Sr^{2+} and Ba^{2+} at a coverage of 4 H_2O/A_{uc} (Figs. EA-4c and EA-4f). A planar pentagonal arrangement of water in the hydration shell of Ba^{2+} at this low water coverage matches the positions of basal oxygens apparently much better than that of Sr^{2+}, which becomes stabilized only at 12–14 H_2O/A_{uc} (Fig. 9c and d). At a coverage of 4 H_2O/A_{uc}, only four first shell waters are shared between Sr^{2+} and mica instead, whereas the fifth water is adsorbed above the Sr^{2+} ion.

Interestingly, at a coverage of 2 H_2O/A_{uc}, the simulated adsorption height of 1.68 Å for Ba^{2+} corresponds very well to experimentally observed interlayer Ba^{2+}–mica distances of 1.64–1.71 Å for Ba-rich trioctahedral micas (Brigatti and Poppi, 1993) and of 1.67 Å for dehydroxylated dioctahedral micas (Keppler, 1990). Although no value should be attached to this fortuitous correspondence itself, it allows an analysis of the coordination environment of Ba^{2+} at a position characteristic for interlayer Ba^{2+} ions. In particular, no satisfactory explanation has been given to Ba–O peaks at 3.20 ± 0.03 Å and 3.56 ± 0.03 Å with coordination numbers of 1.2 and 1.5 observed in an EXAFS study of Ba^{2+} adsorption on montmorillonite (Zhang et al., 2001). The simulated data indicate that these two peaks are due to basal oxygens in the coordination sphere of Ba^{2+} adsorbed in ditrigonal cavities at a height close to 1.68 Å (Fig. 4a). Coordination numbers for these peaks agree very well with the reported ones (Fig. 4b) taking into account that the neglect of double-electron excitation effects (as in the study by Zhang et al., 2001) results in an underestimation of the coordination numbers for Ba^{2+} by 10–15% (D'Angelo et al., 1996b). The simulated Ba–Si/Al distances of 3.7–3.8 Å at this water coverage (Fig. EA-3a) are also in agreement with the reported value of 3.88 ± 0.03 Å (Zhang et al., 2001).

The agreements in peak positions suggest that at the applied experimental conditions (Zhang et al., 2001), Ba^{2+} is specifically adsorbed in ditrigonal cavities in the interlayer space of montmorillonite. Furthermore, the agreement in coordination numbers suggests that Ba^{2+} is not equidistant to the two interlayer montmorillonite surfaces, as otherwise the experimental values of coordination numbers for basal oxygens would be larger by a factor of 2 than the simulated ones for the cleaved surface. This non-equivalence can be rationalized considering, e.g., Ba^{2+} adsorption near a tetrahedral substitution not matched by a tetrahedral substitution on the opposite mineral surface (within the projected area of the first coordination shell of Ba^{2+}), which is very probable because of the low tetrahedral charge of montmorillonite.

3.4. Adsorption of Sr^{2+} and Ba^{2+} at water coverages of 5–14 H_2O/A_{uc}

As can be seen in Figs. 11 and 12, an increase of water coverage beyond the value of 4 H_2O/A_{uc} leads to only small changes in Sr^{2+} and Ba^{2+} adsorption heights, which vary in the ranges 1.89–1.95 Å for Sr^{2+} and 2.12–2.19 Å for Ba^{2+} and equal 1.93 ± 0.02 Å and 2.15 ± 0.03 Å, respectively, at a maximum simulated coverage of 14 H_2O/A_{uc} (Table 1). These changes are related to the advancing completion of the first hydration shells of specifically adsorbed ions,

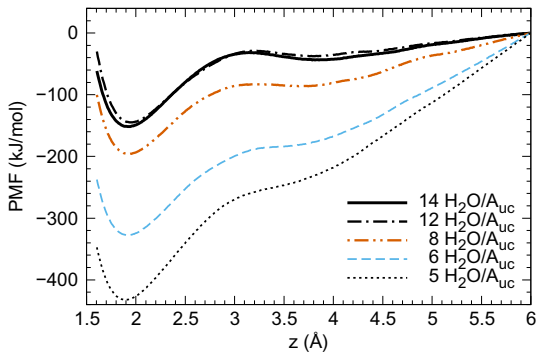

Fig. 11. PMF profiles (kJ/mol) as functions of the distance between Sr^{2+} and mica at the mica–water interface. The position of the basal oxygens of muscovite was set to $z = 0$ Å. PMF profiles were arbitrarily set to zero at $z = 6$ Å.

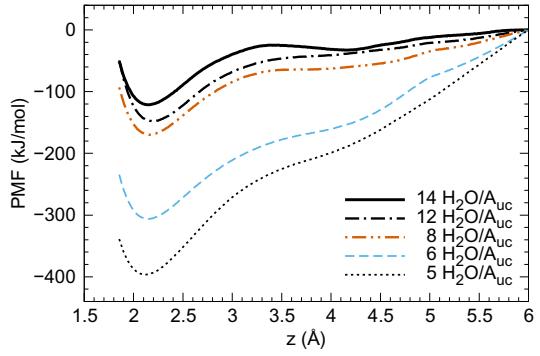

Fig. 12. PMF profiles (kJ/mol) as functions of the distance between Ba^{2+} and mica at the mica–water interface. The position of the basal oxygens of muscovite was set to $z = 0$ Å. PMF profiles were arbitrarily set to zero at $z = 6$ Å.

which is accompanied by adjustments in the hydration shell structure to match the mica surface structure as discussed above. No changes in lateral positions of the adsorbed ions occur as dictated by their favorable coordination with oxygen triads bonded to Al substitutions (Fig. 9).

Outer-sphere adsorption, which is indicated by the second free energy minimum in the calculated free energy profiles, becomes possible upon water adsorption beyond the layer at 4.5 Å at a coverage of 8 H_2O/A_{uc} for Sr^{2+} (Fig. 5a) and upon the formation of the layer at 4.0 Å at a coverage of 14 H_2O/A_{uc} for Ba^{2+} (Fig. 6a). The adsorption heights for outer-sphere adsorbed Sr^{2+} and Ba^{2+} equal 3.9 ± 0.2 Å and 4.17 ± 0.07 Å, respectively, at a coverage of 14 H_2O/A_{uc} (Table 1). At this coverage, the free energy difference $\Delta F_{1,2}$ between the first and the second minima equals 107 ± 7 kJ/mol for Sr^{2+} and 89 ± 13 kJ/mol for Ba^{2+}, whereas the activation energy for a corresponding transformation (the difference between the PMF values at the first maximum and the first minimum) equals 121 ± 3 kJ/mol and 99 ± 10 kJ/mol, respectively (Table 1). Since at this water coverage water layering is largely accomplished in the relevant interfacial region, a transformation from an inner-sphere adsorption complex to an outer-sphere adsorption complex upon a further water adsorption can be dismissed considering the latter prohibitively large values.

A comparison with the corresponding activation energies of 165 kJ/mol (Meleshyn, 2009a) and 144 kJ/mol (Meleshyn, 2009b) for Mg^{2+} and Ca^{2+}, respectively, suggests that adsorption affinities for alkaline earth ions on mica decrease in the sequence $Mg^{2+} > Ca^{2+} > Sr^{2+} > Ba^{2+}$ in agreement with the sequence predicted recently for low dielectric constant solids (Sverjensky, 2006). Considering the value of 83 ± 10 kJ/mol determined experimentally for K^+ desorption from the cleaved mica surface (Raviv et al., 2002), the simulation results further suggest a higher affinity of Ba^{2+} than K^+ to muscovite.

Two recent experimental studies have reported total electron density profiles as well as integrated electron densities for the cleaved muscovite in contact with 0.005 M

Table 1
Characteristics of Sr^{2+} and Ba^{2+} adsorption on the cleaved muscovite surface.

Coverage (H_2O/A_{uc})	0	2	3	4	5	6	8	12	14
h_1^{PMFa} (Å)									
Sr^{2+}	1.12	1.86	1.86	1.88	1.89 ± 0.02	1.93 ± 0.01	1.94 ± 0.02	1.95 ± 0.04	1.93 ± 0.02
Ba^{2+}	1.35	1.68	2.09	2.10	2.12 ± 0.01	2.14 ± 0.02	2.16 ± 0.02	2.19 ± 0.03	2.15 ± 0.03
h_2^{PMFb} (Å)									
Sr^{2+}	–	–	–	–	–	–	3.7 ± 0.2	3.8 ± 0.2	3.9 ± 0.2
Ba^{2+}	–	–	–	–	–	–	–	–	4.17 ± 0.07
$\Delta F_{1,2}$[c] (kJ/mol)									
Sr^{2+}							109 ± 7	106 ± 9	107 ± 7
Ba^{2+}									89 ± 13
E_a[d] (kJ/mol)									
Sr^{2+}							114 ± 8	118 ± 6	121 ± 3
Ba^{2+}									99 ± 10

[a] Height (above the muscovite surface) of the first free energy minimum.
[b] Height (above the muscovite surface) of the second free energy minimum.
[c] Free energy difference between the first and the second free energy minima.
[d] Activation energy for a transformation between inner-sphere and outer-sphere adsorptions (the difference between the free energy values at the first maximum and the first minimum).

(Lee et al., 2007) and 0.01 M (Schlegel et al., 2006) $BaCl_2$ solutions. To derive the coverages and adsorption heights of Ba^{2+}, a best-fit procedure has been used in these papers, which assumes either that the water density at the muscovite–water interface equals that in the bulk water (Schlegel et al., 2006) or that water on Ba^{2+}-exchanged muscovite is distributed in exactly the same way as on the H_3O^+-exchanged muscovite (Lee et al., 2007). Both assumptions are rather crude, as (1) the density of water adsorbed on clay minerals is considerably higher than the bulk water density within the first 5 Å (Mitchell, 1993) and (2) the water distribution on Ba^{2+}-exchanged muscovite (Fig. 6) is predicted in this study to differ from that on H_3O^+-exchanged muscovite (Cheng et al., 2001). Based on the position of the first peak in the total electron density profiles as well as on the discussed empirical structural considerations, a height of ~2 Å (2.02 ± 0.05 Å (Schlegel et al., 2006) or 1.98 ± 0.02 Å (Lee et al., 2007) has been derived from the best-fit modeling of the measured XR data for inner-sphere adsorbed Ba^{2+}, which differs from the simulated value of 2.15 ± 0.03 Å (Fig. 12). A comparison between the experimental and simulated values of the integrated electron densities suggests, however, that in the experimental systems coverages of specifically adsorbed Ba^{2+} could have been significantly lower than 0.5 Ba^{2+}/A_{uc} as used in the present PMF calculations to compensate the negative mica charge.

Indeed, an integration of the total electron density profiles simulated for Ba^{2+} ions specifically adsorbed on the cleaved muscovite at coverages of 0.125–0.5 Ba^{2+}/A_{uc} (Fig. 13a) within ~3.2 Å (first broad solution layer in the study by Schlegel et al. (2006)) or ~3.6 Å (first two rather sharp solution layers in the study by Lee et al. (2007)) from the surface suggests a coverage of ~0.1–0.2 Ba^{2+}/A_{uc} in the experimental systems (Fig. 13b). This coverage is lower than the coverages of 0.3 Ba^{2+}/A_{uc} (Schlegel et al., 2006) and 0.44 Ba^{2+}/A_{uc} (Lee et al., 2007) derived with empirical structural models from XR data for 0.01 M and 0.005 M $BaCl_2$ solutions, respectively. However, it agrees with the experimental observations that a compensation of the muscovite charge by the more strongly adsorbing Ca^{2+} occurs at $CaCl_2$ concentrations above ~0.01 M (Scales et al., 1990) and that the coverage of specifically adsorbed Sr^{2+} at $SrCl_2$ concentration of 0.01 M equals 0.28 ± 0.12 Sr^{2+}/A_{uc} (Park et al., 2006). Furthermore, it can be seen in Fig. 13a that a fit of the interfacial solution structure below ~3.2–3.6 Å by one broad peak or two peaks with similar areas does not necessarily provide an adequate representation of the partial Ba^{2+} electron density profile and may result in a biased Ba^{2+} adsorption height. Therefore, a reconsideration of the empirical structural model used to fit the excellent XR data (Schlegel et al., 2006; Lee et al., 2007) taking into account the presented molecular simulation results as well as an experimental study with a $BaCl_2$ concentration higher than 0.01 M would possibly allow a fairer test of the validity of the simulated adsorption height. A further peak at 4.13 ± 0.08 Å in the total electron density profile for a mixed $BaCl_2$ and fulvic acid solution on muscovite has been assigned to Ba^{2+} in the study by Lee et al. (2007) and corresponds well to a height of 4.17 ± 0.07 Å calculated for outer-sphere adsorbed Ba^{2+} in the present study (Fig. 12).

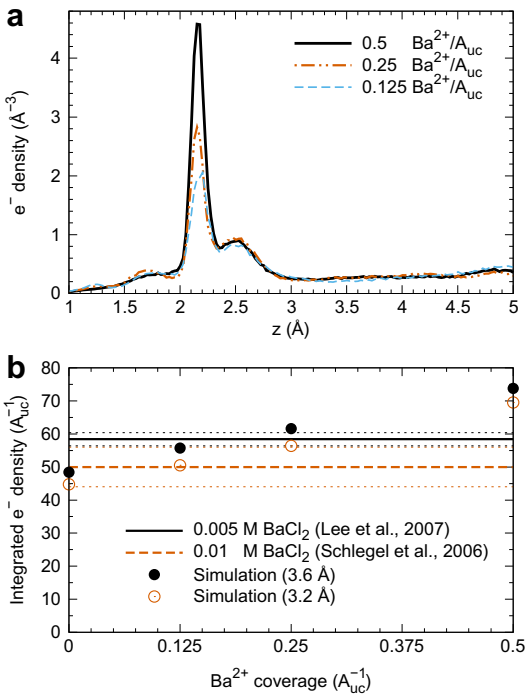

Fig. 13. Total electron density profiles for Ba^{2+} coverages of 0.125, 0.25, and 0.5 Ba^{2+}/A_{uc} as functions of the distance from the muscovite surface (a) and corresponding integrated electron densities (b). To calculate a total electron density profile in (a), the sampled atomic density profiles were multiplied by the corresponding numbers of electrons (1 for hydrogen, 8 for oxygen, 36 for Sr^{2+}, and 54 for Ba^{2+}) and summed. Simulated values in (b) were calculated by integrating the total electron density profiles from 0 up to 3.2 Å or 3.6 Å in accordance with the data from experiments with 0.01 M (Schlegel et al., 2006) or 0.005 M (Lee et al., 2007) $BaCl_2$ solutions, respectively. Experimental values (solid and dashed lines) and their measurement uncertainties (dotted lines) in (b) are shown as lines crossing the whole simulated coverage range, as no exact experimental determination of Ba^{2+} coverage has been carried out. For a coverage of 0 Ba^{2+}/A_{uc}, the value calculated for 1 H_3O^+/A_{uc} at the muscovite–water interface (Meleshyn, 2008b) was used in (b). The position of the basal oxygens of muscovite was set to $z = 0$ Å.

Differently than for Ba^{2+}, both ion-specific and total electron density profiles have been determined for Sr^{2+} on muscovite using RAXR in the excellent study by Park et al. (2006). The observation of two Sr^{2+} peaks at 1.26 ± 0.22 Å and 4.52 ± 0.24 Å with very similar occupancies of 0.28 ± 0.12 Sr^{2+}/A_{uc} and 0.36 ± 0.12 Sr^{2+}/A_{uc} has led to the logical conclusion that outer-sphere adsorption is not weaker than inner-sphere adsorption (Park et al., 2006, 2008). On the contrary, the simulated large free energy difference of 107 ± 7 kJ/mol between these two types of Sr^{2+} adsorption (Fig. 11) supports the common assumption (Stumm, 1992).

In the study by Park et al. (2008), the Gibbs free energy of Sr^{2+} adsorption has been determined to be 32 ± 5 kJ/mol for muscovite covered with a 2–10 μm-thick water

layer. This value is significantly smaller than the calculated activation energy for the transformation between inner-sphere and outer-sphere Sr^{2+} adsorptions of 121 ± 3 kJ/mol, which can be considered as an estimate of the lower limit for the free adsorption energy. However, Park et al., 2006 have also found that Sr^{2+} is stronger adsorbed on muscovite than H_3O^+, which in turn has a comparable adsorption strength as K^+ as discussed by Park et al. (2008). The adsorption free energy of K^+ on the cleaved muscovite surface has been experimentally determined to be 83 ± 10 kJ/mol (Raviv et al., 2002). These observations imply that either the adsorption affinity of Sr^{2+} or that of K^+ or the relation between them must be questioned.

The present simulation confirms the relation between the adsorption affinities of Sr^{2+} and K^+ and suggests that the origin of this contradiction is very likely related to yet another disagreement between the simulated and the experimental inner-sphere adsorption heights of 1.93 ± 0.02 Å and 1.26 ± 0.22 Å (Park et al., 2006), respectively. Notably, the adsorption height of 1.12 Å simulated for Sr^{2+} on dehydrated mica is very close to the value measured experimentally in the presence of water. The only structural analysis of Sr^{2+} in the interlayer space of mica known to the author has been made for dehydroxylated mica (Keppler, 1990) and yielded a Sr^{2+}–mica distance of 1.55 Å as discussed in Section 3.1 (notably, to the author's knowledge, the literature gives only one reference to a naturally occurring Sr-enriched mica (Tischendorf et al., 2007), which is a sodium-strontium paragonite). In an indirect support of the simulated results, the relation between Sr^{2+}– and Ba^{2+}–mica distances in dehydroxylated mica (1.55 Å and 1.67 Å, respectively) is much more similar to the relation simulated on the cleaved muscovite (1.93 ± 0.02 Å and 2.15 ± 0.03 Å, respectively) than to that derived from RAXR and XR studies (1.26 ± 0.22 Å and ~2 Å, respectively).

Accordingly, it can be suggested that the difference in the simulated and the experimental inner-sphere adsorption heights of Sr^{2+} is due to a component or a reaction present in the experimental system but absent in the model system, which stabilizes Sr^{2+} adsorption at the experimentally observed height. Dissolved CO_2 can be considered as such a component, since it has been found to possibly enhance Sr^{2+} adsorption on kaolinite and illite (Cole et al., 2000; Sahai et al., 2000). In this case, surface polymerization or precipitation of strontium carbonate should be assumed to occur on the mica surface, as it is otherwise not clear how Sr^{2+}–carbonate complexation can lead to a strong decrease in Sr^{2+}–mica distance from the energetically most favorable adsorption height of 1.93 ± 0.02 Å to the experimentally observed value of 1.26 ± 0.22 Å. A precipitation of potassium carbonate (Ostendorf et al., 2008) or calcium carbonate (Alcantar et al., 2003) has been proposed as explanation for the observed crystallite growth on the cleaved muscovite surface or between two closely apposed mica surfaces, respectively. Still, the observed equivalent occupancies of inner-sphere and outer-sphere adsorption positions by Sr^{2+} cannot be explained by this mechanism alone, as it should not lead to a strong decrease in the surface density of Sr^{2+} ions positioned at a height of 1.26 ± 0.22 Å from 0.5 Sr^{2+}/A_{uc} necessary to compensate the muscovite lattice charge to the observed 0.28 ± 0.12 Sr^{2+}/A_{uc} (Park et al., 2006).

Therefore, an additional or an alternative modification of the muscovite–water interface should be assumed to occur. A dissociation of hydroxyl groups in the mica lattice as a result of Sr^{2+} adsorption in ditrigonal cavities, which can be suggested as a possible reaction beyond the scope of the present model incorporating muscovite in accordance with the experimentally studied system, may resolve the discussed disagreements. Indeed, the simulated distance between Sr^{2+} adsorbed in a ditrigonal cavity on dehydrated mica (at a height of 1.12 Å) and hydrogen (positioned just below Sr^{2+}) or oxygen of a muscovite hydroxyl group equals 3.36 Å or 3.50 Å, respectively, and is comparable with Sr^{2+}–basal oxygen distances (Fig. 2). It is very likely that this close approach can result in a destabilization of the OH group followed by a hydrogen detachment and either (1) a subsequent protonation of a basal oxygen bonded to an unbalanced (by Sr^{2+}) tetrahedral substitution in accordance with a mechanism proposed by Bhattacharyya (1989) or (2) a subsequent protonation of a water molecule resulting in H_3O^+ ion adsorption above an unbalanced tetrahedral substitution (Meleshyn, 2008b). The total negative lattice charge of muscovite does not change in the first case and becomes even more negative in the second case. Tetrahedral rotations in the ditrigonal cavity, which loses a hydrogen, can be expected to follow a disappearance of hydrogen bridges (Keppler, 1990) and may lead to a decrease in the distance between Sr^{2+} and basal oxygens of the cavity's larger triangle and stabilization of Sr^{2+} adsorption in the ditrigonal cavity.

Such a modification of the muscovite–water interface with one additional positive charge formed there upon one adsorbed Sr^{2+} ion would explain the observation that the surface density of inner-sphere adsorbed Sr^{2+} (0.28 ± 0.12 Sr^{2+}/A_{uc} Park et al., 2006) is by a factor of two lower than that necessary to compensate the muscovite lattice charge (0.5 Sr^{2+}/A_{uc}). Outer-sphere adsorption of 0.25 Sr^{2+}/A_{uc} in excess of the inner-sphere adsorbed 0.25 Sr^{2+}/A_{uc} on the modified muscovite surface may become energetically more favorable in this case, which can be rationalized considering changes in free energy profiles upon changes in the distances between adsorbed cations as discussed for Fig. 1. Note also that the hydroxylation of the muscovite surface can also initiate carbonate ion adsorption as observed by Bhattacharyya (1989), which may be followed by surface polymerization or precipitation of strontium carbonate.

It is important to stress that the model of the process studied in the experiment by Park et al. (2006) states that (1) Sr^{2+} adsorption from (2) aqueous solution occurs on (3) the cleaved muscovite surface. The aim of the present study was to study Sr^{2+} adsorption on the cleaved surface of muscovite according to this experimental model. A study of a deprotonated muscovite, which can be expected to have a very different structure of the basal surface in particular and of the mineral layer in general as discussed above, is beyond the scope of the present study, as the formulated problem in the understanding of Sr^{2+} adsorption on the cleaved muscovite and its possible solution proposed in

the present study should be proven in experiments first. Eventually carrying out classical molecular simulations could follow, as they generally require experimental data on the mineral structure as input information.

4. CONCLUSIONS

On dehydrated mica, Sr^{2+} and Ba^{2+} adsorption in ditrigonal cavities at heights of 1.12 Å and 1.35 Å is preferred due to a match between their hydration radii of 2.60 Å and 2.80 Å, respectively, and the ditrigonal cavity size. In the frame of the used rigid muscovite lattice approach, which conforms to the observed negligible relaxations of <0.04 Å for mineral atoms at the mica–water interface (Cheng et al., 2001), an adsorption of 2–3 H_2O/A_{uc} leads to a displacement of Sr^{2+} and Ba^{2+} ions into positions above tetrahedral substitutions, which allow for a better match between their hydration shells and the muscovite surface as well as for a decreased number of positively charged lattice ions in their first coordination sphere.

At the maximum simulated water coverage of 14 H_2O/A_{uc}, Sr^{2+} and Ba^{2+} are adsorbed as inner-sphere complexes in these positions at heights of 1.93 ± 0.02 Å and 2.15 ± 0.03 Å, respectively. At this coverage, the activation energy for a transformation from an inner-sphere adsorption complex to an outer-sphere adsorption complex equals 121 ± 3 kJ/mol for Sr^{2+} and 99 ± 10 kJ/mol for Ba^{2+}. A comparison with the recently reported activation energies of 165 kJ/mol for Mg^{2+} (Meleshyn, 2009a) and 144 kJ/mol for Ca^{2+} (Meleshyn, 2009b) suggests that adsorption affinities for alkaline earth ions on mica decrease in a sequence $Mg^{2+} > Ca^{2+} > Sr^{2+} > Ba^{2+}$ in agreement with the sequence predicted recently for low dielectric constant solids (which include mica) (Sverjensky, 2006). Taking additionally into account the corresponding activation energy of 83 ± 10 kJ/mol for K^+ (Raviv et al., 2002) results in an adsorption affinity sequence $Mg^{2+} > Ca^{2+} > Sr^{2+} > Ba^{2+} > K^+$ for mica.

A comparison with experimental results for Sr^{2+} adsorption on muscovite (Park et al., 2006, 2008) reveals a strong difference between simulation and experiment in the heights of inner-sphere adsorbed Sr^{2+} as well as in relative stabilities of inner-sphere and outer-sphere adsorbed Sr^{2+} ions. However, the simulation results agree with the common assumption (Stumm, 1992) that inner-sphere adsorption is stronger than outer-sphere adsorption. The present study proposes that a modification of the muscovite–water interface, which is not incorporated in the present simulation model, as a result of Sr^{2+} adsorption in ditrigonal cavities may be responsible for this controversy. This mechanism may prevent a reliable, unbiased experimental determination of adsorption strengths of Sr^{2+} inner-sphere and outer-sphere aqua complexes on mica.

ACKNOWLEDGMENTS

The author thanks to Dr. C. Park for his helpful comments on RAXR study of Sr^{2+} adsorption on mica, two anonymous reviewers and Prof. Neal Skipper for their very helpful comments on the manuscript, and H. Wicke for reading the manuscript.

APPENDIX A. SUPPLEMENTARY DATA

The structure of water at the cleaved mica–water interface. Supplementary data associated with this article can be found, in the online version, at doi:10.1016/j.gca.2009.12.019.

REFERENCES

Alcantar N., Israelachvili J. and Boles J. (2003) Forces and ionic transport between mica surfaces: implications for pressure solution. *Geochim. Cosmochim. Acta* **67**, 1289–1304.

Beaglehole D., Radlinska E. Z., Ninham B. W. and Christenson H. K. (1991) Inadequacy of Lifshitz theory for thin liquid films. *Phys. Rev. Lett.* **66**, 2084–2087.

Bhattacharyya K. G. (1989) Adsorption of carbon dioxide on mica surfaces. *Langmuir* **5**, 1155–1162.

Brigatti M. F. and Poppi L. (1993) Crystal chemistry of Ba-rich trioctahedral micas-1*M*. *Eur. J. Mineral.* **5**, 857–871.

Chen C.-C. and Hayes K. F. (1999) X-ray absorption spectroscopy investigation of aqueous Co(II) and Sr(II) sorption at clay–water interfaces. *Geochim. Cosmochim. Acta* **63**, 3205–3215.

Cheng L., Fenter P., Nagy K. L., Schlegel M. L. and Sturchio N. C. (2001) Molecular-scale density oscillations in water adjacent to a mica surface. *Phys. Rev. Lett.* **87**, 156103.

Cole T., Bidoglio G., Soupioni M., O'Gorman M. and Gibson N. (2000) Diffusion mechanisms of multiple strontium species in clay. *Geochim. Cosmochim. Acta* **64**, 385–396.

D'Angelo P., Notling H.-F. and Pavel N. D. (1996a) Evidence for multielectron resonances at the Sr K edge. *Phys. Rev. A* **53**, 798–805.

D'Angelo P., Notling H.-F. and Pavel N. D. (1996b) Multielectron excitations at the L edges of Ba in aqueous solution. *Phys. Rev. B* **54**, 12129–12138.

Ferrario M., Haughney M., McDonald I. R. and Klein M. L. (1990) Molecular-dynamics simulation of aqueous mixtures: methanol, acetone, and ammonia. *J. Chem. Phys.* **93**, 5156–5166.

Gertner B. J. and Hynes J. T. (1998) Model molecular dynamics simulation of hydrochloric acid ionization at the surface of stratospheric ice. *Faraday Discuss.* **110**, 301–322.

Giese R. F. (1974) Surface energy calculations for muscovite. *Nature* **248**, 580–581.

Jorgensen W. L., Chandrasekhar J., Madura J. D., Impey R. W. and Klein M. L. (1983) Comparison of simple potential functions for simulating liquid water. *J. Chem. Phys.* **79**, 926–935.

Jorgensen W. L., Maxwell D. S. and Tirado-Rives J. (1996) Development and testing of the OPLS all-atom force field on conformational energetics and properties of organic liquids. *J. Am. Chem. Soc.* **118**, 11225–11236.

Keppler H. (1990) Ion exchange reactions between dehydroxylated micas and salt melts and the crystal chemistry of the interlayer cation in micas. *Am. Miner.* **75**, 529–538.

Kim E. B., Faller R., Yan Q., Abbott N. L. and de Pablo J. J. (2002) Potential of mean force between a spherical particle suspended in a nematic liquid crystal and a substrate. *J. Chem. Phys.* **117**, 7781–7787.

Kuwahara Y. (2001) Comparison of the surface structure of the tetrahedral sheets of muscovite and phlogopite by AFM. *Phys. Chem. Miner.* **28**, 1–8.

Lee S. S., Nagy K. L. and Fenter P. (2007) Distribution of barium and fulvic acid at the mica–solution interface using in-situ X-ray reflectivity. *Geochim. Cosmochim. Acta* **71**, 5763–5781.

Meleshyn A. (2008a) Two-dimensional ordering of water adsorbed on mica surface at room temperature. *J. Phys. Chem. C* **112**, 14495–14500.

Meleshyn A. (2008b) Aqueous solution structure at the cleaved mica surface: influence of K^+, H_3O^+, and Cs^+ adsorption. *J. Phys. Chem. C* **112**, 20018–20026.

Meleshyn A. (2009a) Potential of mean force for Mg^{2+} at the cleaved mica–water interface. *J. Phys. Chem. C* **113**, 12946–12949.

Meleshyn A. (2009b) Potential of mean force for Ca^{2+} at the cleaved mica–water interface. *J. Phys. Chem. C* **113**, 17604–17607.

Mitchell J. K. (1993) *Fundamentals of Soil Behaviour*. Wiley, New York.

Moreau G., Helm L., Purans J. and Merbach A. E. (2002) Structural Investigation of the aqueous Eu^{2+} ion: comparison with Sr^{2+} using the XAFS technique. *J. Phys. Chem. A* **106**, 3034–3043.

Ohtaki H. and Radnai T. (1993) Structure and dynamics of hydrated ions. *Chem. Rev.* **93**, 1157–1204.

Ostendorf F., Schmitz C., Hirth S., Kühnle A., Kolodziej J. J. and Reichling M. (2008) How flat is an air-cleaved mica surface? *Nanotechnology* **19**, 305705.

Park C., Fenter P., Nagy K. L. and Sturchio N. C. (2006) Hydration and distribution of ions at the mica–water interface. *Phys. Rev. Lett.* **97**, 016101.

Park C., Fenter P., Sturchio N. C. and Nagy K. L. (2008) Thermodynamics, interfacial structure, and pH hysteresis of Rb^+ and Sr^{2+} adsorption at the muscovite (001)−solution interface. *Langmuir* **24**, 13993–14004.

Pashley R. M. and Israelachvili J. N. (1984) DLVO and hydration forces between mica surfaces in Mg^{2+}, Ca^{2+}, Sr^{2+}, and Ba^{2+} chloride solutions. *J. Colloid Interface Sci.* **97**, 446–455.

Ramos S., Neilson G. W., Barnes A. C. and Capitan M. J. (2003) Anomalous X-ray diffraction studies of Sr^{2+} hydration in aqueous solution. *J. Chem. Phys.* **118**, 5542.

Raviv U., Laurat P. and Klein J. (2002) Time dependence of forces between mica surfaces in water and its relation to the release of surface ions. *J. Chem. Phys.* **116**, 5167–5172.

Sahai N., Carroll S. A., Roberts S. and O'Day P. A. (2000) X-ray absorption spectroscopy of strontium(II) coordination: II. Sorption and precipitation at kaolinite, amorphous silica, and goethite surfaces. *J. Colloid Interface Sci.* **222**, 198–212.

Scales P. J., Grieser F. and Healy T. W. (1990) Electrokinetics of the muscovite mica–aqueous solution interface. *Langmuir* **6**, 582–589.

Schlegel M. L., Nagy K. L., Fenter P., Cheng L., Sturchio N. C. and Jacobsen S. D. (2006) Cation sorption on the muscovite (001) surface in chloride solutions using high-resolution X-ray reflectivity. *Geochim. Cosmochim. Acta* **70**, 3549–3565.

Skipper N., Chang F.-R. and Sposito G. (1995) Monte Carlo simulation of interlayer molecular structure in swelling clay minerals. 1. Methodology. *Clays Clay Miner.* **43**, 285–293.

Seward T. M., Henderson C. M. B., Charnock J. M. and Driesner T. (1999) An EXAFS study of solvation and ion pairing in aqueous strontium solutions to 300 °C. *Geochim. Cosmochim. Acta* **63**, 2409–2418.

Stumm W. (1992) *Chemistry of the Solid–Water Interface*. Wiley, New York.

Sverjensky D. A. (2006) Prediction of the speciation of alkaline earths adsorbed on mineral surfaces in salt solutions. *Geochim. Cosmochim. Acta* **70**, 2427–2453.

Tischendorf G., Förster H.-J., Gottesmann B. and Rieder M. (2007) True and brittle micas: composition and solid–solution series. *Miner. Mag.* **71**, 285–320.

Wang F. and Landau D. P. (2001) Efficient, multiple-range random walk algorithm to calculate the density of states. *Phys. Rev. Lett.* **86**, 2050–2053.

Wang J., Kalinichev A. G., Kirkpatrick R. J. and Cygan R. T. (2005) Structure, energetics, and dynamics of water adsorbed on the muscovite (001) surface: a molecular dynamics simulation. *J. Phys. Chem. B* **109**, 15893–15905.

Xu L. and Salmeron M. (1998a) Effects of surface ions on the friction and adhesion properties of mica. *Langmuir* **14**, 2187–2190.

Xu L. and Salmeron M. (1998b) An XPS and scanning polarization force microscopy study of the exchange and mobility of surface ions on mica. *Langmuir* **14**, 5841–5844.

Yeh I.-C. and Berkowitz M. L. (1999) Ewald summation for systems with slab geometry. *J. Chem. Phys.* **111**, 3155–3162.

Zhang P.-C., Brady P. V., Arthur S. E., Zhou W.-Q., Sawyer D. and Hesterberg D. A. (2001) Adsorption of barium(II) on montmorillonite: an EXAFS study. *Colloids Surf. A* **190**, 239–249.

Zhou C. and Bhatt R. N. (2005) Understanding and improving the Wang–Landau algorithm. *Phys. Rev. E* **72**, 025701(R).

Associate editor: James Kubicki